

OFDR-Based Distributed Sensing and Fault Detection for Single- and Multi-Mode Avionics Fiber-Optics

Roger G. Duncan, Brian J. Soller, Dawn K. Gifford, Steven T. Kreger, Ryan J. Seeley,
Alexander K. Sang, Matthew S. Wolfe, and Mark E. Froggatt
*Luna Technologies, A Division of Luna Innovations Incorporated, 3157 State St., Blacksburg,
VA 24060*

I. INTRODUCTION

Short-length optical communications networks such as those employed in avionics and aerospace applications are in need of frequent assessment of link health. Precise localization and identification of cracks and breaks, as well as an accurate assessment of loss due to fiber bends, splices, and connectors is critical to maintaining signal integrity along the link.

Traditionally, optical time domain reflectometry (OTDR) is employed for installation- and maintenance-based inspection of fiber systems. However, in many respects traditional OTDR is not well-suited for avionics applications, which are typically dominated by short runs of optical fiber (less than 100 m). This is due to the technological limitations of launch and event dead-zone inherent to OTDR, which can be a significant percentage of the total link length for the short-run networks encountered in avionics. Likewise alternate techniques, such as optical low-coherence reflectometry (OLCR), have limited applicability to avionics fiber-optics.

Herein we introduce an optical frequency domain reflectometry (OFDR) technique and its applications in single- and multi-mode avionics fiber-optics. Multiple measurement examples within the avionics field not currently supported by conventional test tools or methods are provided, including high-resolution fault detection and distributed sensing along unaltered standard telecommunications grade optical fiber with millimeter spatial resolution. The utility of this technique as a health monitoring tool for existing and new avionics fiber-optic networks is discussed.

II. FAULT DETECTION

II.A. Measurement Technique

In this work, OFDR is used to measure the Rayleigh scatter of a fiber under test (FUT).^{1,2} The measurement network is shown in Figure 1. Light from an external-cavity tunable laser source (TLS) is split between the reference and measurement arms of an interferometer. In the measurement path, the light is further split to interrogate a length of fiber under test (FUT) and return the reflected light. Another coupler then recombines the measurement and reference fields. A polarization beam splitter (PBS) and a polarization controller (PC) are used to split the reference light evenly between two orthogonal polarization states. As the laser is linearly tuned in optical frequency the interference between the measurement field and these two polarization states is then recorded at detectors labelled S and P. This polarization diversity technique is used in OFDR to mitigate signal fading due to polarization misalignment of the interfering measurement and reference fields. Not shown in the figure is an auxiliary interferometer used to trigger data acquisition in equal optical frequency increments and a portion of the tunable laser wherein a gas-cell is used to monitor the absolute wavelength of the tunable laser.

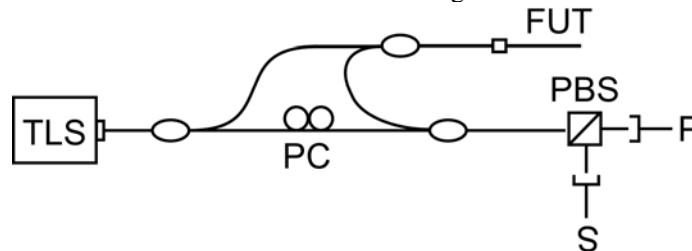


Figure 1: Optical network used for sensor array interrogation.

Once the complex reflection coefficient is obtained in the frequency domain, the reflectivity as a function of length is obtained via the Fourier transform (see reference 3 for details). In all testing described herein, a commercial off the shelf (COTS) OFDR-based optical backscatter reflectometer (OBR) manufactured by Luna Technologies, a division of Luna Innovations Incorporated, is used to perform the measurements.

II.B. Fault Detection and Network Diagnostic Examples

The principle strengths of OFDR are the achievable spatial resolution (millimeter-level two-point spatial resolution is achievable over 2 km of optical fiber) and the achievable sensitivity (-130 dB). These characteristics make OFDR uniquely suited to fault detection and identification. Figure 2 displays the results of a measurement of the reflectivity of a 300 m length of standard single-mode fiber. There are two bends in the fiber, each with 2.5 cm radius. The bends show up as loss events in much the same way as they would appear on an OTDR trace. The two-point spatial resolution over the full length of the measurement is 800 μm with zero dead-zone.

Figure 3 shows measurement results of the reflectivity of a sample network consisting of a 50/50 coupler with a bad splice in one output arm. Note that at the location of the bad splice, a very weak reflectivity is recorded along with an associated drop in the ‘noise’ level on either side of the splice. The apparent noise is in fact the Rayleigh scatter signature in the fiber. The apparent noise is in fact the Rayleigh scatter signature in the fiber. Any insertion loss event is registered as a drop in the scatter level at the location of the event. Note also that high resolution nature of the measurement makes it possible to identify the location of the fused-tapered coupler due to an associated drop in the backscatter level.

Many of the short-run applications encountered on aircraft utilize multi-mode fiber of different types and sources in different spectral regions. Thus it is imperative that avionics test instrumentation be equipped to deal with the different fiber and component types encountered in avionics systems.

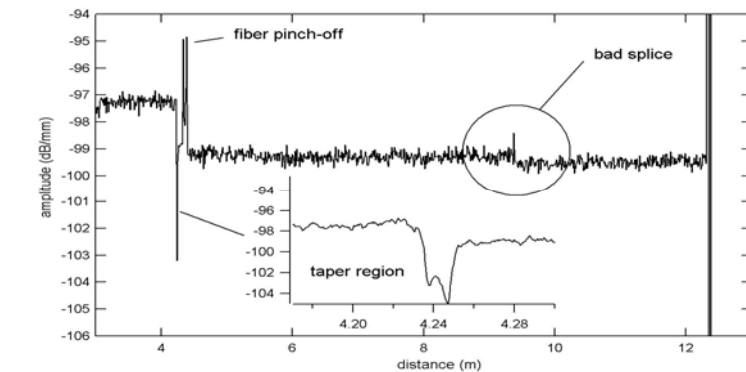


Figure 3: Reflectivity of a 50/50 coupler with a bad splice in one of the output arms. The areas of ‘noise’ are the Rayleigh scatter signature of the fiber.

converter used is a proprietary in-house design. However, any single- to multi-mode converter that excites the higher order modes appropriately would suffice.

The lighter, dotted curve represents a measurement of the multi-mode fiber with no mode converter—the single- and multi-mode fibers are simply spliced together. In this case, the insertion loss at the 5 mm bend is not recorded, likely due to the poor mode-filling conditions in the multi-mode fiber. The darker curve is a measurement

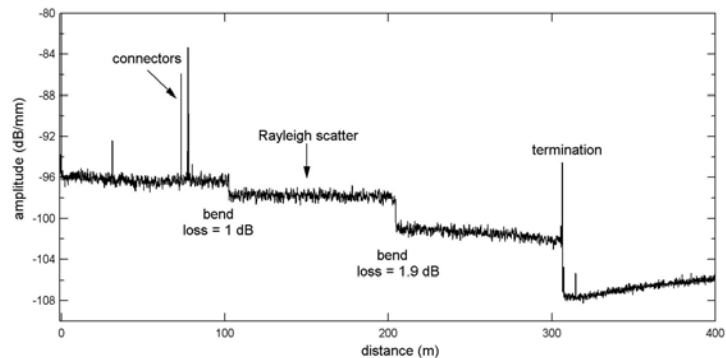


Figure 2: Reflectivity of a 300 m run of single-mode fiber at 1550 nm with tight bends at two locations. The distributed loss between 200 m and 300 m is caused by spooling the fiber on an 8 cm diameter mandrel. The two-point spatial resolution here is 800 μm .

with the different fiber and component types encountered in avionics systems.

In order to properly test a fiber system containing multi-mode fiber, the single-mode fiber that comprises the system described here must be appropriately coupled to the multi-mode system. This is accomplished by the use of a mode converter designed to fill the higher order modes of the multi-mode fiber.

Figure 4 (left) displays the results of the reflectivity of a fiber system comprised of single-mode fiber coupled to 62.5 μm core multi-mode fiber using a spatial mode converter. The mode

with the mode converter in the network. The loss intrinsic to the mode coupling process is visible in the data at a distance of about 2 m. Note that in this case, the reflection due to the bend and the insertion loss at the location of the bend are both readily apparent.

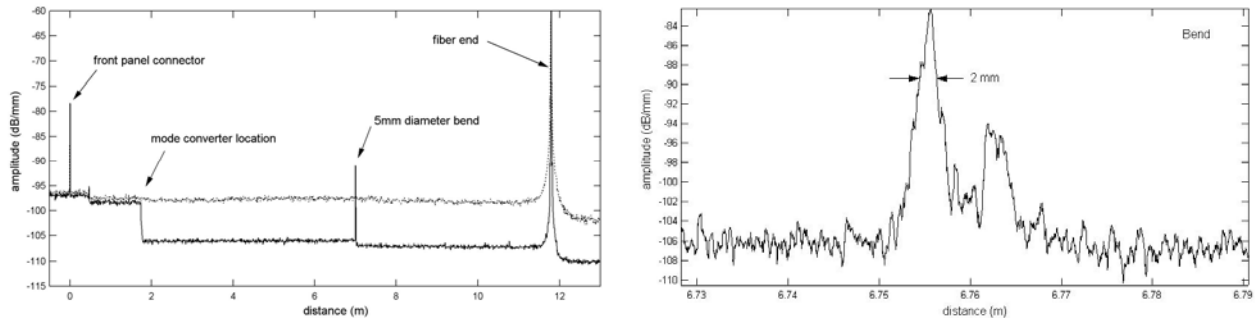


Figure 4: Left – Signal trace of a network containing multi-mode fiber. The light, dotted curve is a measurement of the system with single- and multi-mode fiber connected using a conventional splice. For the darker curve, a mode converter, which populates the higher order fiber modes, is used to connect the two different fiber types, resulting in improved performance. Right – An expanded view of the 5 mm diameter bend. The width of the bend signature is 2 mm. The two-point spatial resolution of the multi-mode measurement is less than 300 μm .

Figure 4 (right) shows an expanded view of the region containing the bend. Note that the high resolution nature of the coherent technique makes it possible and practical to discriminate between a bend and, say, a bad splice.

The achievable resolution in the multi-mode system is somewhat degraded by the increased modal dispersion. However, over the lengths under consideration in this paper, the achieved spatial resolution remains in the sub-millimeter regime.

Figure 5 is intended to demonstrate the high-resolution diagnostic capabilities of the OFDR technique. The figure displays the reflectivity of a ‘good’ avionics fiber-optics air-gap connector and the same air-gap connector with a break induced in the fiber exiting the rubber boot on the far side of the connection. The break is clearly visible even though there is only approximately 39.5 mm between the break and the fiber interface reflection. The two-point spatial resolution in this measurement example is again less than 1 mm allowing for clear detection of the ‘bad’ connector in the presence of a strong reflection.

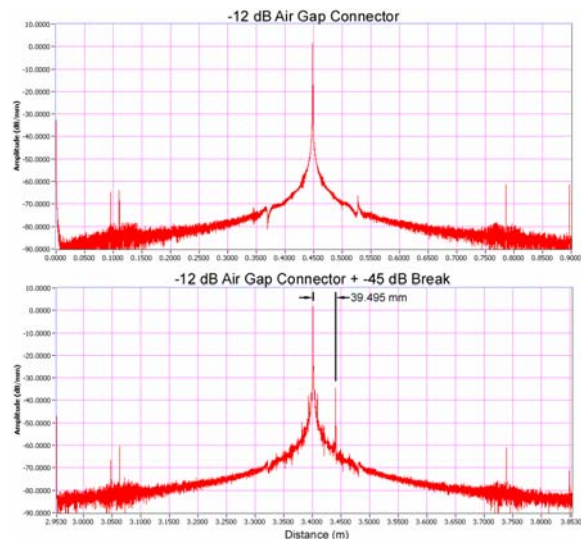


Figure 5: Measurement of a ‘good’ (top) and a ‘bad’ (bottom) air-gap connector.

II.C. Applicability to Longer Networks

Though the primary concern of this paper is short-haul avionics fiber-optic networks, it is perhaps relevant to demonstrate the applicability of this measurement technique to performing diagnostics on longer optical fiber networks. Figure 6 (left) shows a measurement of an approximately 2 km fiber spool with three FC/APC connections at the end. The Rayleigh scatter of the fiber is clearly visible above the noise floor, which sits at approximately -130 dB. Figure 6 (right) shows a zoomed-in view of the connectors at the end of the spool. A macro-bend and its associated loss is clearly visible 17 cm after the second connector. The two-point spatial resolution achieved here was 800 μm . It is also perhaps significant to note that the acquisition time for this data was less than 100 ms, which is substantially faster than that achievable with competing measurement techniques.

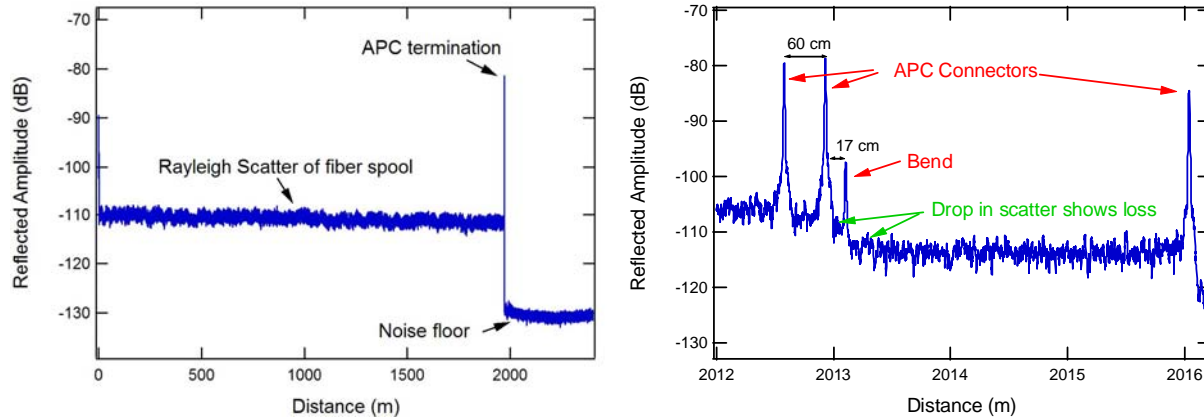


Figure 6: Left – Reflected amplitude vs. distance for a 2 km fiber spool with three FC/APC connectors at the end. Right – Zooming-in shows the connector reflections, a bend, and the insertion loss associated with the bend.

III. DISTRIBUTED SENSING WITH UNALTERED FIBER

III.A. Measurement Technique

Rayleigh scatter in optical fiber is caused by random fluctuations in the index profile along the fiber length that are the result of minor imperfections in the fiber manufacturing process. For a given fiber, the scatter amplitude as a function of distance is a random but static property of that fiber and can be modeled as a long, weak fiber Bragg grating with a random period. Changes in the local period of the Rayleigh scatter caused by an external stimulus in turn cause changes in the locally reflected spectrum. This spectral shift can then be calibrated to form a distributed sensor.

Similarly to the fault-detection application described above, OFDR is used to measure the complex reflection coefficient of a fiber as a function of wavelength. The Rayleigh scatter as a function of length is obtained via the Fourier transform. A sensor is formed by first measuring and storing the Rayleigh scatter signature of the fiber at a baseline state. The scatter profile is then measured in a perturbed state. The scatter profiles from the two data sets are then compared along the entire fiber length in increments of Δx ; each segment represents a discrete sensing element.

When a segment of fiber experiences a change in state, the reflected spectrum from that segment shifts proportionally. To determine the amount of spectral shift, a complex cross-correlation is performed between reference data and measurement data for each fiber segment. Any change in state manifests as a shift in the correlation peak. Therefore, to make a distributed measurement one simply measures the shift in the cross-correlation peak for each segment along the fiber. Effectively, with the Rayleigh scatter sensing technique, the fiber itself becomes the sensor.⁴⁻⁸

III.B. Distributed Strain Measurement Examples

Distributed strain measurements can have many applications on board aircraft. An example of a distributed strain measurement that benefits from the high-spatial resolutions afforded by this technique is a measurement of the strain profile of a multi-mode fiber in a four-fiber heavy duty cable under twist, as shown in Figure 7. The induced twist resulted in a highly variable level of tensile strain on the fiber. The average and maximum strains monitored on the 4 m length of cable rises in an approximately linear fashion with the twist rate. Using the fiber manufacturer's guideline for the maximum safe tensile stress of 20 kpsi to ensure a 40 yr installation lifetime, the suggested maximum twist rate for this cable is 3.3 full turns per meter. Monitoring fiber strain in this direct manner allows the fiber cable installer to inspect for dangerous stress concentrations post installation and is highly preferable to relying on estimates derived from mechanical modeling.

Figure 8 shows the basic setup of an experiment designed to assess the utility of this technique for performing high-accuracy distributed strain measurements. Here, strain was precisely induced by mounting a translation stage with micrometer drive on a rail and clamping communications grade single mode fiber onto the stage and on a distant point on the rail. In the apparatus a micrometer with ± 1 micron resolution moved a stainless steel linear bearing stage mounted to an aluminum rail. Fusion splice protectors were used to grip the fiber; the splice protectors were clamped down to the linear stage and rail. The fiber had a lead length of approximately 638 meters; the total effective gage length, consisting of the fiber between the clamps, was 990 mm. Using the translation stage, the fiber segment was elongated in 40 micron increments

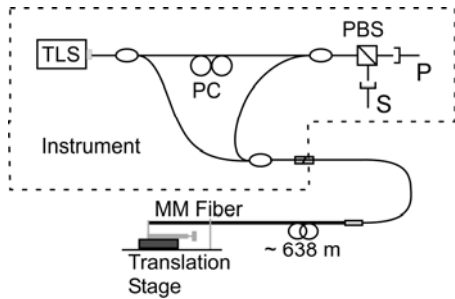


Figure 8: Experimental set-up.

measured parameters. This is not surprising as the strain relationship for fused silica optical fibers has been observed to be extremely linear, with negligible hysteresis in acrylate coated samples over the strain ranges experienced herein, consistent with the very hard, non-ductile nature of fused silica. The fit residuals, which can also be seen in Figure 9 (right, bottom), are presented to give an indication of accuracy. The values compare favorably to the estimated strain uncertainty stemming from the resolution of the micrometer of $\pm 1.0 \mu\epsilon$.

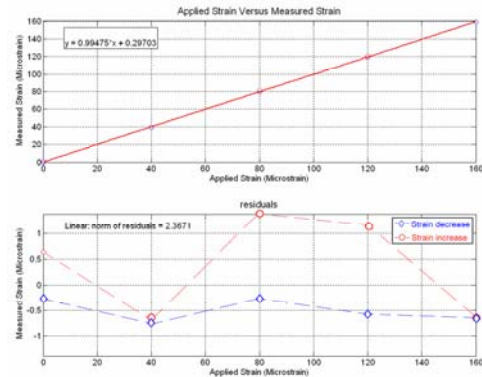
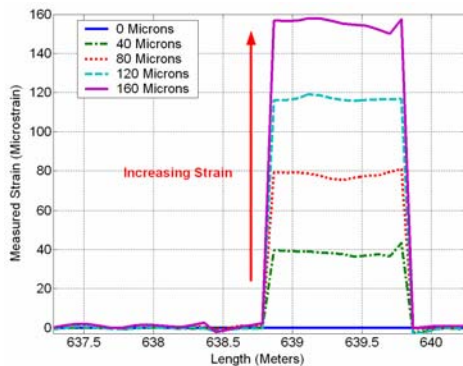


Figure 9: Left – Measured strain as a function of distance along the fiber. Right (top) – Mean of measured strain over which strain was applied vs. applied strain. Right (bottom) – The fit residuals.

III.C. Distributed Temperature Measurement Examples

Similarly, distributed temperature measurements may be useful in a number of on-board applications such as watching for over-temperature conditions in fuel tanks or brake linings, monitoring potential icing conditions on flight surfaces, as well as detecting overheated components in the fiber communications and control network. A demonstration of distributed temperature sensing in standard single-mode fiber is shown in Figure 10. The fiber is

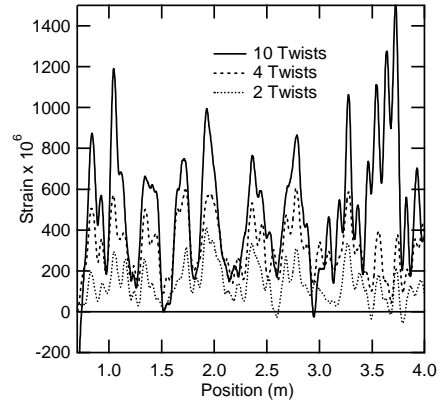


Figure 7: Distributed strain profile in a multi-mode fiber as a function of twist number.

between 0 and 160 μm , inducing a step change in strain.

Figure 9 (left) shows the measured strain as a function of distance in the up-sweep of the experiment. A rise in strain is noticed at position 638.8 m that returns to a null state at position 639.7 m. This is consistent with the known effective gage length of 990 mm.

Figure 9 (right, top) is a plot of the measured strain as a function of applied strain. A slope of 0.995 was calculated, indicating a high level of correlation between the calculated and

measured parameters. This is not surprising as the strain relationship for fused silica optical fibers has been observed to be extremely linear, with negligible hysteresis in acrylate coated samples over the strain ranges experienced herein, consistent with the very hard, non-ductile nature of fused silica. The fit residuals, which can also be seen in Figure 9 (right, bottom), are presented to give an indication of accuracy. The values compare favorably to the estimated strain uncertainty stemming from the resolution of the micrometer of $\pm 1.0 \mu\epsilon$.

looped into two containers into which ice water and heated water is poured. A reference scan is taken before the introduction of the water and compared to successive traces taken several minutes apart. In successive scans the region of fiber in the cold water bath is stable because ice maintains the temperature near the freezing point, whereas the region of fiber in the hot water bath gradually loses heat to the surrounding environment.

IV. CONCLUSION

We have shown the OFDR technique to be a useful and practical tool for diagnosing and troubleshooting the types of fiber networks found in avionics applications. The achievable spatial resolution in combination with the backscatter-level sensitivity gives this technique distinct advantages over competing methods. Unique attributes include zero dead-zone, the ability to unambiguously identify different types of failure modes encountered in short-haul single- and multi-mode fiber networks, and the capability to perform distributed sensing with unaltered single- or multi-mode telecommunication grade optical fiber. These advantages speak to the efficacy of OFDR-based instrumentation in providing multiple capabilities within the avionics field not currently supported by conventional test tools or methods.

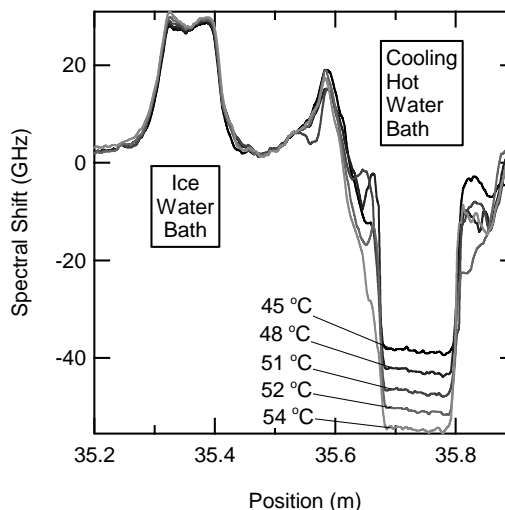


Figure 10: Spectral shift vs. position for the water baths. The spectral shift of the Rayleigh scatter can be linearly scaled to temperature shift.

V. REFERENCES

1. Soller, B., Gifford, D., Wolfe, M., and Froggatt, M., "High resolution optical frequency domain reflectometry for characterization of components and assemblies," *Opt. Express* 13, 666 (2005).
2. Oberson, P., Huttner, B., Guinnard, O., Guinnard, L., Ribordy G., and Gisin, N., "Optical frequency domain reflectometry with a narrow linewidth fiber laser," *IEEE Photon. Technol. Letters* 12, 867 (2000).
3. Soller, B., Gifford, D., Wolfe, M., and Froggatt, M., "Polarization resolved measurement of Rayleigh backscatter in fiber-optic components," in *National Fiber Optic Engineer's Conference, OSA Technical Digest Series* (Optical Society of America, Washington, DC), paper NWD3 (2005).
4. Kreger, S., Gifford, D., Froggatt, M., Sang, A., Duncan, R., Wolfe, M., Soller, B., "High-Resolution Extended Distance Distributed Fiber-Optic Sensing Using Rayleigh Backscatter," *SPIE International Symposium on Smart Structures and Materials, Proc. SPIE* 6530-64 (2007).
5. Kreger, S., Gifford, D., Froggatt, M., Soller, B., and Wolfe, M., "High resolution distributed strain or temperature measurements in single- and multi-mode fiber using swept-wavelength interferometry," *OFS 18 Technical Digest, Cancun, Mexico, Oct 2006*, paper ThE42.
6. Sang, A., Duncan, R., Kreger, S., Froggatt, M., "High-Resolution Extended Distanced Distributed Strain Measurements Using Swept-Wavelength Interferometry," *Proceedings of EPRI's 3rd Increased Power Flow Conference* (2006).
7. Froggatt, M., Soller, B., Gifford, D., and Wolfe, M., "Correlation and keying of Rayleigh scatter for loss and temperature sensing in parallel optical networks," *OFC Technical Digest*, paper PDP 17, 2004.
8. Froggatt, M., and Moore, J., "High resolution strain measurement in optical fiber with Rayleigh scatter," *Appl. Opt.*, 37, 1735 (1998).